IEEE Access
Multidisciplinary ⋮ Rapid Review ⋮ Open Access Journal

Received May 5, 2021, accepted May 13, 2021, date of publication May 27, 2021, date of current version June 7, 2021.

Digital Object Identifier 10.1109/ACCESS.2021.3084215

Multi-Objective Takeoff Time Optimization Using Cellular Automaton-Based Simulator

KATSUHIRO SEKINE[1], TOMOAKI TATSUKAWA[2], (Member, IEEE), ERI ITOH[3,4], AND KOZO FUJII[2], (Member, IEEE)

[1]Department of Industrial Management and Engineering, Tokyo University of Science, Tokyo 125-8585, Japan
[2]Department of Information and Computer Technology, Tokyo University of Science, Tokyo 125-8585, Japan
[3]Air Traffic Management Department, National Institute of Maritime, Port and Aviation Technology, Tokyo 182-0012, Japan
[4]Electronic Navigation Research Institute, Chofu 82-0012, Japan

Corresponding author: Tomoaki Tatsukawa (tatsukawa@rs.tus.ac.jp)

This work was supported by the Ministry of Education, Culture, Sports, Science and Technology (MEXT), as Exploratory Challenge 2 (ID: hp190163) on Post-K Computer (Construction of Models for Interaction Among Multiple Socioeconomic Phenomena, Sub-Issue: Model Development and its Applications for Enabling Robust and Optimized Social Transportation Systems).

ABSTRACT Although schedule design has further potential to reduce airline operation costs and flight delay, the effectiveness of the globally optimal schedule design integrating air traffic flow has not been discussed thus far. This paper presents a global multi-objective takeoff time optimization to design efficient flight schedules that lead to minimal congestion and provide sufficient resilience against traffic problems. NSGA-II is adopted as the multi-objective optimization technique in this study. The objective functions include minimization of the total arrival delay and total fuel consumption because these are key performance indicators of air traffic management (ATM). The design variable used in this study is the takeoff time offset of each flight landing at the Tokyo International Airport. 607 design variables were used in this study. The range of the design variables was ± 300 s to investigate the effect of a minor variation in the takeoff time. A cellular automaton-based model was utilized to simulate the interaction of the flights with each other. The results of the simulations demonstrated that the obtained optimal solutions could drastically reduce the total arrival delay and total fuel consumption by 1500 min and 80 tons, respectively. The spacing adjustments of one of the optimum flight schedules, in comparison to the original flight schedule, were reduced by 80% in the en-route and terminal airspaces. Additional analyses suggest that it is preferable to have longer takeoff time intervals for flights originating from the same point during congestion hours than those during non-congestion hours. This indicates that the optimization of ground movements in airports improves the efficiency of air traffic operations.

INDEX TERMS Air traffic control, air traffic management, cellular automaton, flight scheduling, ground holding program, NSGA-II, schedule design.

I. INTRODUCTION

Air traffic demand has rapidly grown across the world in previous decades [1]. Despite the sharp reduction in revenue passenger kilometers due to COVID-19, the air traffic demand is expected to recover in the next 4 years, albeit with uncertainty [2]. The International Civil Aviation Organization (ICAO) has proposed a unique operational concept for air traffic management (ATM), so-called trajectory-based operations (TBO), to meet the increasing demand for air traffic [3]. This involves the management of the trajectories of all flights from their departure to arrival. The implementation of TBO requires collaborations among the industries, academia and governments, which was encouraged by the promotion of industrial and academic techniques in local areas, such as the Next-Generation Air Transportation System (NextGen) [4] in the U.S., Single European Sky Air Traffic Management (SESAR) [5] in European countries, and Collaborative Actions for Renovation of Air Traffic Systems (CARATS) [6] in Japan. Various studies have been conducted as part of these programs in collaboration with ATM stakeholders to enhance ATM performance.

Air traffic flow management (ATFM) is one of the most crucial operations in the ATM framework. ATFM generally involves strategic regulation of flights to capacity-constrained airports or flights that will pass through capacity-constrained

The associate editor coordinating the review of this manuscript and approving it for publication was Camelia Delcea.

airspace areas at a national scale. Traffic regulation at airports with limited capacity has been widely discussed in previous studies and is commonly referred to as the ground holding problem (GHP). Several GHP mathematical programming methods have been developed to determine the optimal allocation of ground delays and minimize the expected cost of the overall delays [7]–[13]. Existing models are able to decide the allocation of ground delays once at the beginning of the planning period, assuming that the all airspace capacities are known [7], [8]. Those models have been updated to incorporate the uncertainties in the airspace capacity [9], [11], [13], and to develop dynamic decision making by utilizing the updated capacity information during the GHP planning period [10], [12]. Machine learning (ML) techniques have recently been implemented by using historical data of actual operations to improve the accuracy in the ground delay prediction [14]–[17]. These studies have investigated the effect of various factors, related to the traffic demand and weather conditions on the GHP, understood the mechanism underlying GHP, and predicted necessary ground delays. Those mathematical and machine learning models have focused on delaying the takeoff time using a reactive approach.

Developing optimal flight schedules beforehand to adjust the takeoff time falls under a different paradigm. Flight scheduling traditionally comprises of the following four stages: (1) schedule design, (2) fleet assignment (3) route construction, and (4) crew pairing [18]. These stages are closely associated with each other, which indicates that disturbances in any of the stages often affects the other stages negatively. As noted in [19], disruptions are mainly categorized into flight delays, flight cancellation, fleet availability, and airport disruption. To minimize the overall probability of the aforementioned disruptions, several researchers have developed robust flight scheduling models integrating two or three of the flight scheduling stages. Sherali *et al.* (2010) proposed an integrated fleet assignment and schedule design model in which the characteristics of passenger demand were considered [20]. Jiang and Barnhart (2013) developed a robust schedule design model, which dynamically scheduled the departure time in response to the fluctuations in demand in a de-banking environment [21]. Pita *et al.* (2014) proposed the fleet assignment and schedule design model to minimize the overall costs in air transportation network, and they implemented network welfare analysis [22]. Cadarso and Celis (2017) presented an airline planning model integrating schedule design, fleet assignment, and passenger use, considering the stochastic demand value and uncertain operational conditions, to minimize the number of passengers who miss the connecting flight [23]. Faust *et al.* (2017) proposed the schedule design and aircraft maintenance routing model to maximize the profit of medium-sized point-to-point airlines with a homogeneous fleet while considering the demand for the various fare classes [24]. Kenan *et al.* (2018) developed an integrated scheduling model, including schedule design, fleet assignment, and aircraft routing, in consideration of delay propagation and deadhead flights under the uncertainty in demand [25]. Wei *et al.* (2019) proposed an integrated optimization approach for schedule design and fleet assignment focusing on the potential revenue obtained from the customer satisfaction, attractiveness of each itinerary, and passenger repurchasing determinants [26].

These robust flight scheduling studies, however, applied heuristic optimization approaches, although the flight scheduling problem is NP-Hard in nature. This suggests that the obtained flight schedules are not necessarily globally optimal. Further, assuming a linearity, the objective function formulated with a single weighted linear sum was a minimization of the overall costs and/or maximization of the overall profit. This indicates that the relationships among the terms in the function had not been quantitatively investigated. In the field of ATM research, including flight scheduling, there have been few studies that conducted multi-objective optimization with meta-heuristic approaches and analyzed the obtained optimal solutions in detail with the data-mining approaches [27]–[29], although significant design knowledge can be potentially extracted from those optimal or sub-optimal solutions. Furthermore, optimal schedules obtained in the related works were not created in consideration of the weather conditions and air traffic flow although they have a large impact on flight delay, which is one of the four disruption types [19]. The other three disruptions, namely, flight cancellation, fleet availability, and airport disruption, occur as irregular events, complicating the mitigation of thereof probabilities, and are thereby often managed through recovery-based approaches [19], [30], [31]. In contrast, flight delays, whose causes vary depending on the locations [32], could relatively be reduced using a proactive approach such as simulation-based approaches and delay analyses, including the aforementioned GHP studies. Therefore, it would be of interest (1) to evaluate the effectiveness of the multi-objective flight schedule global optimization combined with air traffic flow simulation and (2) to analyze the optimal solutions to enhance our understanding of the factors contributing to ground holding operation and flight scheduling.

This study aims to develop efficient and environmentally friendly flight schedules with minimal congestion. We utilized a multi-objective optimization technique based on NSGA-II [33]. NSGA-II is one of the most used genetic algorithms (GA). The objective functions include (1) minimization of the total arrival delay and (2) minimization of the total fuel consumption, which correspond with the demands of the customers and airlines, respectively. The difference between the scheduled and actual takeoff time of each flight arriving at Tokyo International Airport (RJTT) was used as the design variable. The number of design variables used in this study was 607. The design variables were varied by ± 300 s to investigate the effect of the minute takeoff time difference in consideration of takeoff time error with a few minutes in the flight schedules. Although true optimality is not guaranteed as the obtained sub-optimal solutions are computed based dependent on the GA variant, this

study emphasizes the importance of analyzing the obtained sub-optimal solutions for efficient schedule design through the data-mining approaches. A cellular automaton-based simulator was adopted to simulate air traffic flow because it consists of various complex rules and is heavily dependent on the installed equipment and weather.

The remainder of this paper is organized as follows. Section II provides a brief overview of the simulator used in this study. The existing simulator, which has been constructed by the author's research group, is based on the cellular automaton model. Section III describes the problem statement for the multi-objective optimization of the schedule design. Section IV presents the computational configuration of the simulator. The optimization framework used to solve the multi-objective schedule design problem is mentioned in Section II and Section III. Section V analyzes and discusses the results of a case study wherein the proposed multi-objective optimization model is adopted for inbound traffic at the RJTT. Finally, our conclusions are then presented in Section VI.

II. MODEL DESCRIPTION AND FORMULATION

Air traffic flow has been simulated previously in demand capacity balancing (DCB) studies, congestion analysis, and other ATM-related studies, using mathematical models, such as queue [34]–[37], the differential equation [38]–[43], and network [44]–[47]. Many strategic ATM concepts based on these models have been proposed, and these concepts enable a low computational cost. However, mathematical and theoretical models are not necessarily able to explain air traffic flow precisely because they are based several complex rules and are strongly affected by aircraft facilities and the weather. Agent-based modeling is a different approach that has also been utilized in the field of ATM by several researchers [29], [48]–[51]. Although multiagent models can describe phenomena in detail, it is difficult to develop a highly accurate model due to the high degree of freedom required. The cellular automaton model is similar to the multiagent-based model, but is simpler. As mentioned by Sun *et al.* [52], the cellular automaton model is computationally friendly compared with the Eulerian flow theory and PDE models, which are theoretical models. Thus, we focused on a cellular automaton model that can simulate complex phenomena by following simple rules.

A. CELLULAR AUTOMATON

A cellular automaton model (CA) is a discrete computational model [53] that consists of a regular grid of cells, with each cell existing in one of the finite number of states, such as 0 and 1. The state of each cell is updated after each discrete time interval in accordance with simple rules.

Several CA models [54]–[60] have been proposed to analyze air traffic flow. Kim *et al.* [54] proposed a two-dimensional CA model to demonstrate an airborne self-separation system by describing aircraft that move in all directions within adjacent airspaces. Yu *et al.* [55] and He *et al.* [56] utilized a one-dimensional CA model that can simulate the aircraft landing process for scheduling aircraft landing time in real time. Jin Wang and Hui Gong [57] and Lim and Zhong [58] adopted a two-dimensional CA model for en-route airspace by combining optimization techniques, to search for flight paths that avoid prohibited airspace, restricted airspace, and dangerous airspace. Enayatollahi and Atashgah [59], [60] constructed a two-dimensional CA model considering a standard terminal arrival route (STAR) to investigate the impact of weather on delays and to optimize the flight path following performance-based navigation (PBN). Most studies have not focused on constructing a CA model in the global airspace, such as Japan and Europe, but in terminal airspace or specific en-route airspace.

To address this gap, we propose a one-dimensional CA model with step back movement (SBCA) that was constructed considering Tokyo International Airport (RJTT) [61] and Japan [62]. Our objective was to contribute to the production of a fast-time simulation and optimization toolset in which ATM stakeholders can quickly and easily change airspace and routes for verifying new ATM concepts. Therefore, the unique characteristics of SBCA is its ability to model air traffic flow with only a few parameters, simple input files, and simpler rules than those followed in previous related studies. Our models [61], [62] were updated according to the aircraft characteristics using the Base of Aircraft Data (BADA) [63] and data on international flights arriving at RJTT.

B. BASIC RULE

SBCA consists of three basic rules that utilize two parameters, d BD, and aircraft speed s. d is the minimum in-trial separation between aircraft, and BD is the step-back distance. s [cells/timestep] is the ground speed of each aircraft. s is calculated following the BADA model [63] according to the status of each aircraft, such as climb, cruise, and descent. Then, air speed closest to the position of each aircraft is added to the s calculated based on the BADA model. An aircraft travels according to the rules listed below (Fig. 1).

1) If there is no aircraft in the front for a distance of d cells, then the aircraft moves forward by s cells (step forward).
2) If there are one or more aircraft in the front within a distance of d cells, and there is no aircraft in the rear for

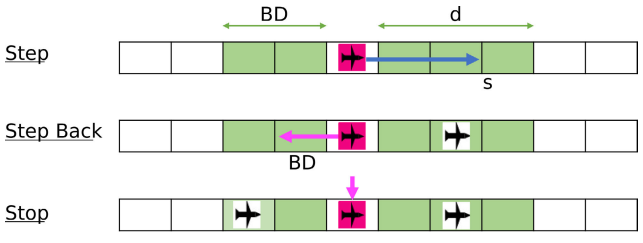

FIGURE 1. Basic rules.

a distance of *BD* cells, then the aircraft moves backward by *BD* cells (step back).

3) If there are one or more aircraft in the front within a distance of *d* cells and in the rear within a distance of *BD* cells, then the aircraft remains in its current position (stop).

Rules (2) and (3) correspond to spacing adjustments, such as vectoring and holding. Although Rule (3) temporarily allows for the introduction of a conflict, by violating the separation minima *d*, the aircraft to which Rule (3) is applied will stop by Rule (2) or step back by Rule (3) in the next time step, thereby solving the conflict immediately.

C. CASE STUDY DATA DESCRIPTION-TOKYO INTERNATIONAL AIRPORT

This study focuses on the domestic and international flights arriving at the Tokyo International Airport (RJTT). Tokyo International Airport (RJTT is the busiest airport in Japan, and the fourth busiest airport in the world, which witnessed 85,408,975 passengers in 2017 [64].

The airport makes use of four runways: a set of parallel north-south runways (34L/16R and 34R/16L) and two southwest-northeast crosswind runways (22/04 and 23/05). Two major runway configurations (see Fig. 2) are operated depending on the wind direction. At the northerly operating wind runway, an aircraft arrives at either runway 34L or runway 34R, and a departing aircraft takes off from runway 05 or runway 34R, depending on their origin/destination airports (see Fig. 2(a)). Basically, the northbound traffic utilizes runway 34R for both departure and arrival, while the southbound traffic makes use of runway 05 and runway 34L for departure and arrival, respectively. The southerly operated wind runway, at which an aircraft arrives at runway 16L and 16R (see Fig. 2(b)) was started in 2020. In this operation, departure aircraft to south-western destination takeoff from runway 22, and the others depart from runway 16L and runway 16R in combination with the arrival aircraft.

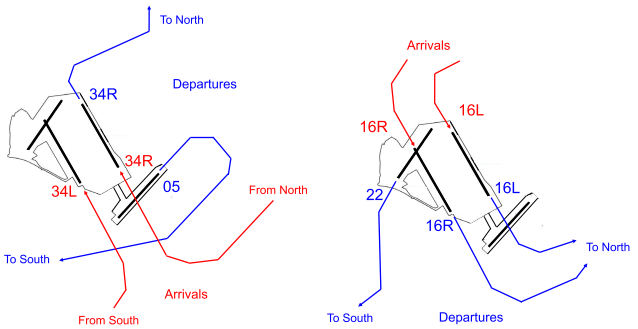

(a) North wind operation (b) South wind operation

FIGURE 2. Runway configuration of departures (blue lines) and arrivals (red lines) at RJTT.

Climate and seasonal fluctuations change runway configurations. According to the operational records between 6:00 AM and 11:00 PM for the years from 2016 to 2018, the northerly wind operation accounted for 70% of the total operations, indicating a larger rate over execution of the southerly wind operation. Based on these statistics, this paper focuses on the northerly wind operation.

Figure 3 shows the flight paths to RJTT, which is indicated by a black square in Fig. 3. The flight paths are created by connecting the flight paths written in flight plan (FP) of the flights arriving at RJTT in a single day. The flights landing on 34R do not affect the flights landing on 34L because the flight paths ending at 34L, depicted by red lines in Fig. 3, and the flight paths ending at 34R, depicted by blue lines in Fig. 3, are independent. SBCA is constructed between confluence points. Each domestic flight departs from a domestic airport in Japan, while each international flight starts at the designated fix. The scheduled takeoff or departure time is extracted from the time written in the first line in each FP. These flights merge into other routes continuously until they arrive at RJTT. The first-come-first-serve protocol is applied to each merging point as a confluence rule. If more than two aircraft arrive at a confluence point, the flight that is scheduled to arrive at RJTT earlier is prioritized over the other. This is the procedure followed in simulating air traffic flow between taking off and landing.

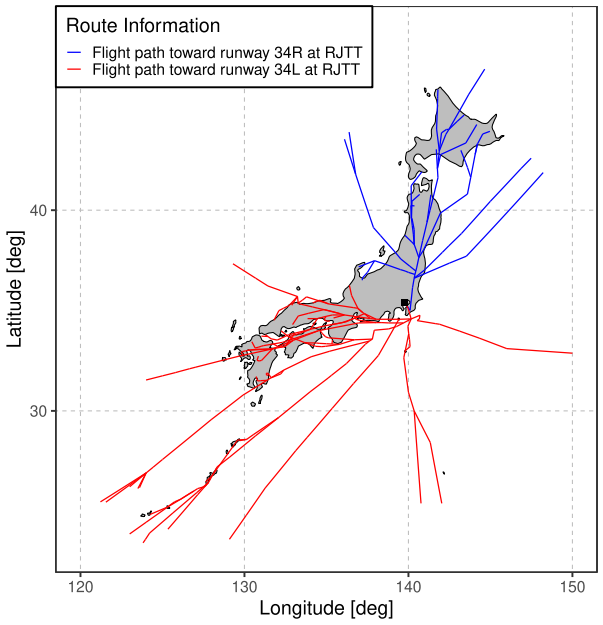

FIGURE 3. Flight path to Tokyo International Airport (RJTT).

The meso-scale model grid point value (MSMGPV), provided by the Japan Meteorological Agency, is employed to study the impact of weather. The data were collected by the Research Institute for Sustainable Humanosphere, Kyoto University (http://database.rish.kyoto-u.ac.jp/index-e.html). The data include atmospheric properties such as wind and temperature mapped on a three-dimensional grid. These data are published every 3 hours. The grid points are located after 0.125° of longitude, 0.1° of latitude, and 50–100 hPa of

pressure of altitude. In this study, the data of the grid point closest to the aircraft were used to add the wind speed to the true air speed in the traveling direction.

III. DESCRIPTION AND FORMULATION OF THE OPTIMIZATION PROCESS

A. MULTI-OBJECTIVE OPTIMIZATION

The multi-objective evolutionary algorithm (MOEA), as shown in Fig. 4, is used to find the optimal solution of the optimization problem. The MOEA is capable of calculating multiple optimal solutions in a single simulation run due to its population-based approach, as shown in Fig. 4. The MOEA creates initialized populations, which are also known as ''parent solutions'' and serve as design variables. The algorithm then assigns fitness values by calculating the objective function's values. Certain populations are selected to reproduce the new populations, which are termed as ''offspring solutions.'' The crossover and mutation techniques are used in the reproduction phase. These are the ways to stochastically generate new solutions from an existing population, imitating the crossover that happens during sexual reproduction in biology. Thus, a certain number of solutions are selected from the offspring solutions to form the parent solutions of the next generation. This process is iterated until the end of the number of generations in MOEA. Finally, non-dominated solutions, so-called ''pareto front,'' are obtained as the result of MOEA.

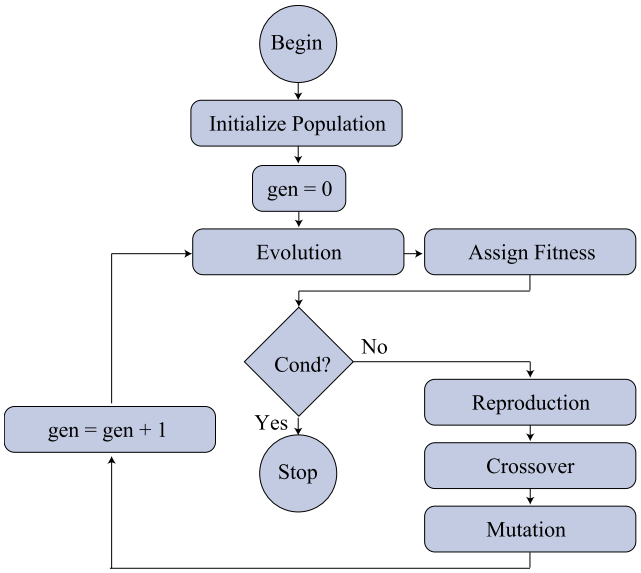

FIGURE 4. Flowchart of the general multi-objective evolutionary algorithm (MOEA).

B. PROBLEM SETTING

We attempted to develop a flight schedule with minimal congestion and fuel consumption in this study. Thus, the objective functions are (1) minimization of the total arrival delay and (2) minimization of the total fuel consumption. The optimization problem is mathematically defined by using the parameters listed in Table 1 as follows:

TABLE 1. Definitions of the parameters used in the optimization problem.

Parameter	Definition
N_f	the number of flights in a day's schedule
N_d	the number of delayed flights in N_f
$T_{SA_{f_i}}$	the scheduled landing time of flight f_i
$T_{AA_{f_i}}$	the actual landing time of flight f_i
$T_{SD_{f_i}}$	the scheduled takeoff time of flight f_i
$T_{AD_{f_i}}$	the actual takeoff time of flight f_i
$F_{i,j}$	the fuel consumption of f_i per time step [kg/timestep]
$O_{SD_{f_i}}$	takeoff time offset of flight f_i
O_l	lower bound of takeoff time offset
O_u	upper bound of takeoff time offset

$$\begin{aligned} &\text{minimize} \sum_{i=1}^{N_d}(T_{AA_{f_i}} - T_{SA_{f_i}}) \\ &\sum_{i=1}^{N_f}\sum_{j=T_{AD_{f_i}}}^{T_{AA_{f_i}}} F_{i,j} \\ &\text{subject to } O_l \le O_{SD_{f_i}} \le O_u \end{aligned} \tag{1}$$

Arrival delay is defined as the difference between the actual landing time ($T_{AA_{f_i}}$) and the scheduled landing time ($T_{SA_{f_i}}$) written in the flight plans. Total arrival delay is calculated by summing up the arrival delay of each flight, f_i, to the number of delayed flights, N_d ($i \in 1, 2, \cdots, N_d$). The taxi time durations at the departure and arrival airports are not accounted for in the simulation. Therefore, the arrival delay for each flight is calculated by subtracting the scheduled landing time from the actual landing time. With respect to fuel consumption, the performance table files (PTF) of BADA are utilized to calculate the amount of the in-flight fuel burned based on the aircraft type. In the PTF, the nominal fuel consumption [kg/min] is described in each FL between FL0 and approximately FL430 based on the status of the aircraft (i.e., climb, cruise, or descent). These values are converted into the values using time step in SBCA [kg/timestep]. Thus, the total fuel consumption is calculated by summing up the fuel consumption per time step, $F_{i,j}$, from the actual departure time ($T_{AD_{f_i}}$) to the actual arrival time ($T_{AA_{f_i}}$) for all flights, N_f ($i \in 1, 2, \cdots, N_f, j \in T_{AD_{f_i}}, \cdots, T_{AA_{f_i}}$). In addition, we investigated the effects of the takeoff time difference on the arrival time and fuel consumption by fixing the arrival time and offsetting the takeoff time. Thus, the design variable of the simulation is the takeoff time offset of each flight ($O_{SD_{f_i}}$) between the lower bound (O_l) and upper bound (O_u).

IV. COMPUTATIONAL CONDITIONS

Table 2 shows the parameter setting of the optimization framework. Multi-objective air traffic flow optimization is conducted by using the non-dominated sorting genetic algorithm II (NSGA-II) [33]. This algorithm has proven to be an effective and efficient multi-objective search technique in various engineering applications. The design variables are the

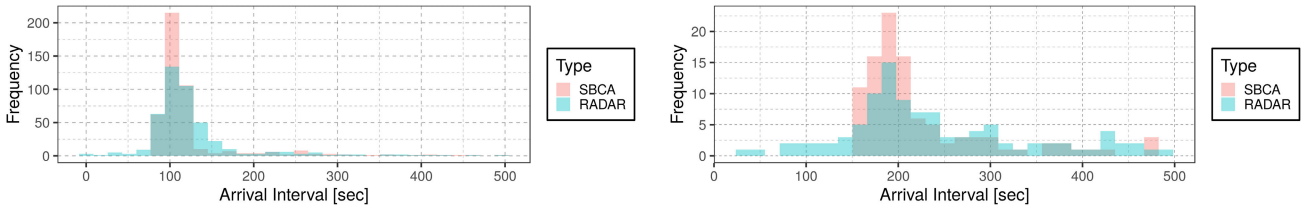

(a) Runway 34L (b) Runway 34R

FIGURE 5. Arrival interval.

TABLE 2. Optimization configuration.

MOEA	NSGA-II
# of Population size	200
# of Generation	200
# of design variable (# of flights)	607
Range of offset [s]	[-300, 300]
Trials	1

TABLE 3. Parameter setting in SBCA.

Parameter			Value
Date			15th, November, 2016
# of flights landing at 34R			140
# of flights landing at 34L			467
# of departure airport			51
# of starting fix for international flights			17
# of routes constructed for SBCA			119
l_x: Length of a cell in the lateral direction			70 [m]
l_y: Length of a cell in the vertical direction			20 [m]
Δt: Timestep			1 [s]
d	34R arrivals	climb	5 [NM] / (l_x/1852)
		cruise	16 [NM] / (l_x/1852)
		descent	10 [NM] / (l_x/1852)
	34L arrivals	climb	5 [NM] / (l_x/1852)
		cruise	7 [NM] / (l_x/1852)
		descent	6 [NM] / (l_x/1852)
BD	34R arrivals		5 [NM] / (l_x/1852)
	34L arrivals		2 [NM] / (l_x/1852)

takeoff time offsets of each flight arriving at RJTT. Therefore, the number of design variables is equal to the number of flights arriving at RJTT, which is equal to 607. The design variables vary between -300 s and $+300$ s to investigate the impact of a minute difference in the takeoff time on the arrival delay and fuel consumption. The value interval for the decision variables is 1 s corresponding to the time step in SBCA, Δt, as shown in Table 3.

As described in Section II, SBCA is the rule-based deterministic simulator. Therefore, the computational parameters of SBCA listed in Table 3 determine the behavior of each aircraft. The simulation was performed on 11/15/2016, which is one of the nominal dates when the north wind operation was applied at RJTT. The MSMGPV data were collected on that date. The number of flights landing on runways 34R and 34L were 140 and 467, respectively. There are 51 departure airports, which include 49 domestic airports, the Taiwan Taoyuan International Airport (RCTP), and the Taipei Songshan Airport (RCSS). The flights departing from these airports follow the climb phase specified by the BADA model. However, the other international flights start with the cruise phase at 17 designated fixes. 119 unique flight paths were used to construct the SBCA in this simulation. The cell length was 70 m in the lateral direction and 20 m in the vertical direction. A CA analysis with a time step of 1 second was then implemented to update the state of each flight. The values of d and BD were adjusted on the basis of a previous study [61] to account for the arrival interval of the actual traffic data (CARATS Open Data [65]) on 11/15/2016 at runways 34L and 34R (see Fig. 5). These values determine the in-trail separation in each flight phase and virtually control the arrival capacity at RJTT. 40,000 simulations were performed by using the parameters listed in Table 2 and Table 3 to calculate the optimal takeoff time and thereby minimize the total arrival delay and total fuel consumption.

V. RESULTS AND DISCUSSION

This section discusses the results of the numerical simulations from the four perspectives mentioned in Section V-A (i.e., the validation result), Section V-B (i.e., the arrival delay and fuel consumption), Section V-C (i.e., the attribution of the reduction of the arrival delay and fuel consumption), and Section V-D (i.e., the takeoff time adjustments). Section V-A focuses on generating trust in our model by comparing the nominal simulation result with the radar track by calculating four metrics. After the validation, Section V-B focuses on the impact of the objective functions of the multi-objective optimization by quantifying the benefits of controlling the minute variations in the takeoff time. Analyzing the optimal solutions in detail, along with optimizing the schedule design, is crucial for efficient ground delay operation and flight scheduling. Therefore, Section V-C analyzes the attribution of the successful reduction in the arrival delay and fuel consumption. Section V-D discusses the efficient control of the takeoff time by analyzing the design variables and their effects.

A. VALIDATION RESULT

Figure 6 presents a comparison between the simulation result and the radar track. Four comparison metrics are calculated. Additional distance is the difference between the scheduled flight path and the actual traveling distance. Arrival delay is the difference between the scheduled landing time and actual

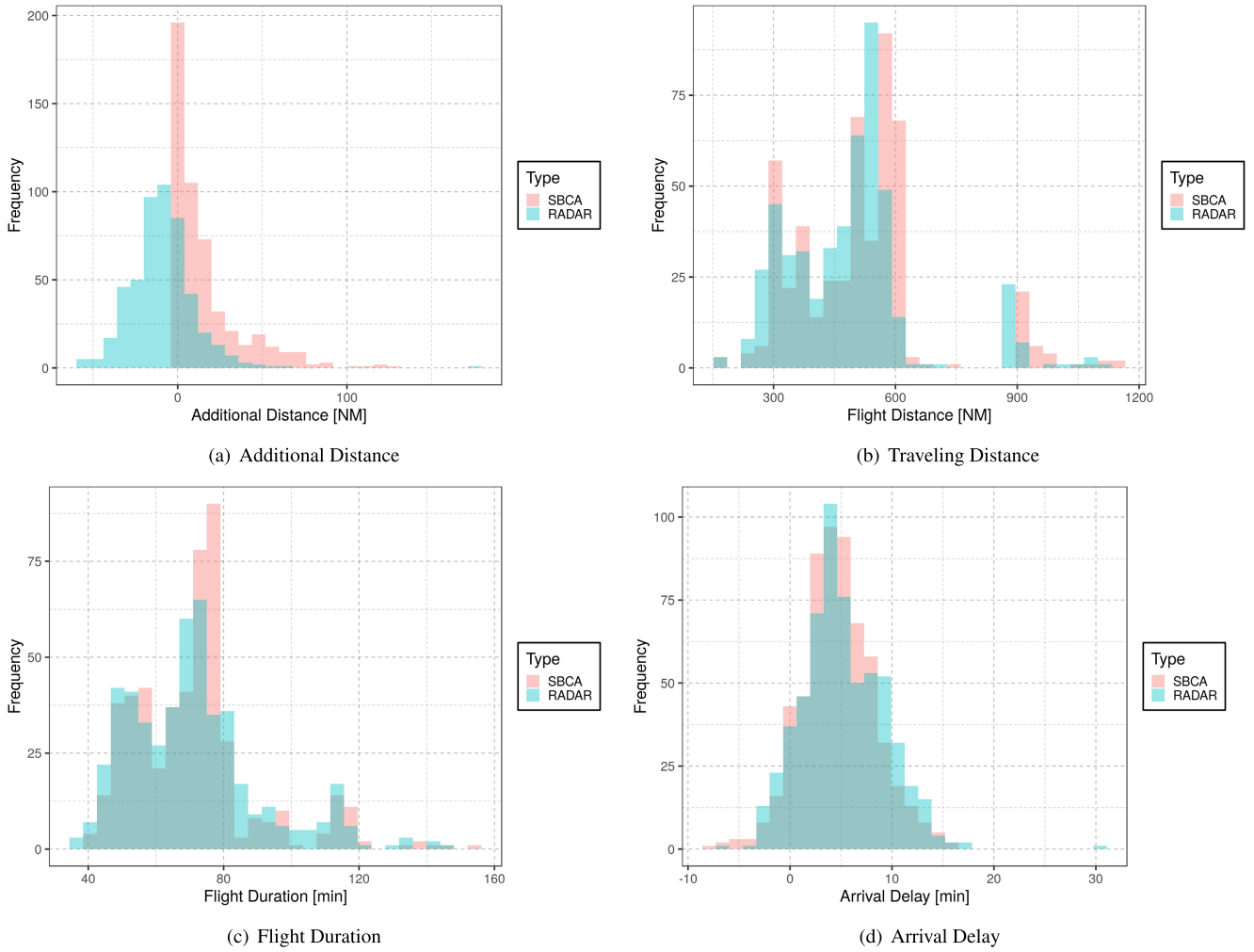

(a) Additional Distance

(b) Traveling Distance

(c) Flight Duration

(d) Arrival Delay

FIGURE 6. **Calculated metrics for validation.**

landing time. Considering that the statistical distributions of the calculated metrics are quite close, it is implied that our model can capture the dynamics of individual flights accurately. With respect to the additional distance in Figure 6(a), some flights in the radar track take a shortcut. Although our model cannot represent the shortcut mechanism, the other calculated metrics of our model are in agreement with those of the radar track, as shown in Figs. 6(b), 6(c), and 6(d). Further comparative analyses will be provided in our future work.

B. ANALYZING ARRIVAL DELAY AND FUEL CONSUMPTION

Figure 7 depicts the objective results of the original schedule and the solutions obtained by using the multi-objective evolutionary algorithm MOEA. From the engineering perspective, this figure enables to analyze the tradeoff between the objective functions and the degree of improvement of the optimal solution from the original solution. The horizontal axis represents the total arrival delay, whereas the vertical axis represents the total fuel consumption. The blue circles represent the solutions obtained by using the MOEA. A total of 40,000 solutions are generated because the number of generations and populations are 200 each. The red circles are non-dominated solutions, while the green square is the solution corresponding to the original schedule. A total of 18 non-dominated solutions were obtained in the current set of simulations. The non-dominated solutions are superior to the solution corresponding to the original schedule (hereinafter referred to as the ''original solution''), as shown in Fig. 7. The total arrival delay and total fuel consumption decreased by approximately 1500 min and 80 tons, respectively. As shown in Table 4, averaged values of the reduced arrival delay and fuel consumption are approximately 100 s and 130 kg, respectively. Thus, the current optimization technique successfully generates flight schedules that minimize delay and fuel consumption. Further, the values of objective functions with non-dominated solutions are almost the same although there is a quite weak tradeoff relationship between the total arrival delay and total fuel consumption, as shown in Fig. 7. The degree of similarity should be investigated in the

TABLE 4. Representative solutions of the results of multi-objective optimization.

Calculated Metrics	Original Solution	Minimum Delay Solution	Minimum Fuel Solution
Total arrival delay [min]	2940.63	1427.88	1451.07
Averaged arrival delay [sec]	320.796	220.239	226.729
Total number of delayed flights [ac]	550	389	384
Percentage of the number of delayed flights [%]	90.61	64.09	63.26
Total fuel consumption [t]	3236.63	3164.35	3157.82
Averaged fuel consumption [kg]	5332.18	5213.09	5202.33

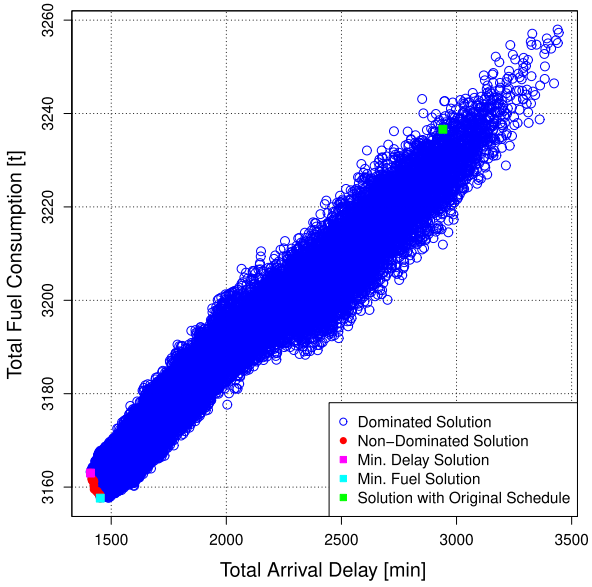

FIGURE 7. Scatter plot in objective function space.

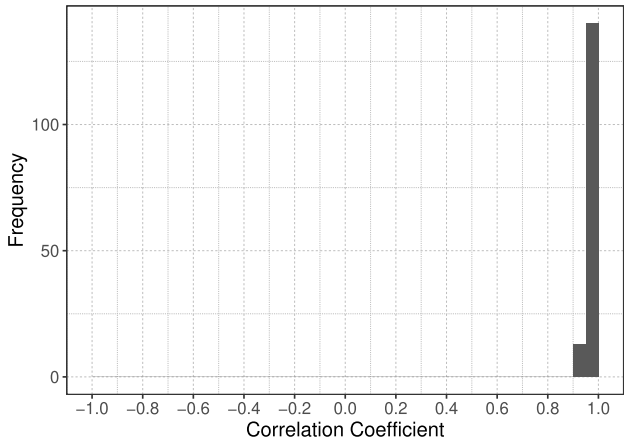

FIGURE 8. Histogram of the correlation coefficient for all pairs of the non-dominated solutions.

space of the design variables, as well as that of the objective functions.

Figure 8 depicts a histogram of the correlation coefficient for all pairs of the non-dominated solutions. As the number of obtained non-dominated solutions is 18, the total number of pairs is 153 ($_{18}C_2$). The pairs are distributed between 0.90 and 1.00, with most being located between 0.95 and 1.00, as shown in Fig. 8. This indicates the existence of a strong positive correlation between each non-dominated solution. Thus, each non-dominated solution is similar in the space of the design variables, as well as the objective space. This result suggests that the appropriate adjustment of the takeoff time contributes to the reduction of both the arrival delay and fuel consumption. Thus, these two objective functions can be replaced by one objective function by considering the minute takeoff time difference to be a design variable in the problem setting of the multi-objective optimization.

There is a significant difference between the original solution and the non-dominated solutions, as shown in Figs. 7 and 8. However, the non-dominated solutions are identical to the original solution in the objective space and the design variables space. Therefore, we compared the original solution with one of the non-dominated solutions. The impact of the total arrival delay and total fuel consumption were both accounted for while choosing the non-dominated solutions. As shown in Table 4, the averaged arrival delay and averaged fuel consumption values of the non-dominated solutions was approximately 6 s and 10 kg, respectively. These values indicate that the impact of fuel consumption is greater than that of the arrival delay from customers' and airlines' perspectives. Therefore, we selected the solution that provided minimum total fuel consumption (hereinafter referred to as "minimum fuel solution"), which is indicated by the light blue square in Fig. 7.

Figure 9 depicts the arrival delay of each flight. The horizontal and vertical axes represent the arrival delay and

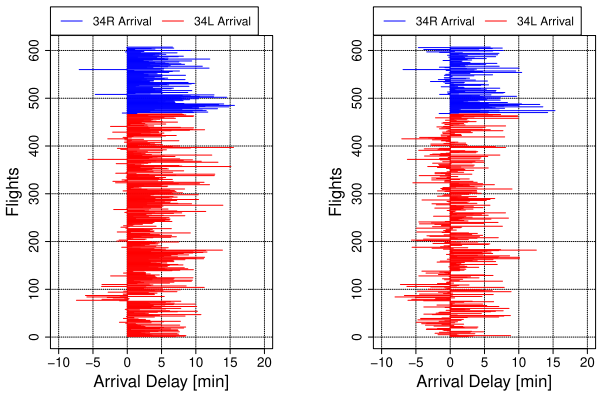

(a) Original Solution (b) Minimum Fuel Solution

FIGURE 9. Arrival delay of each flight.

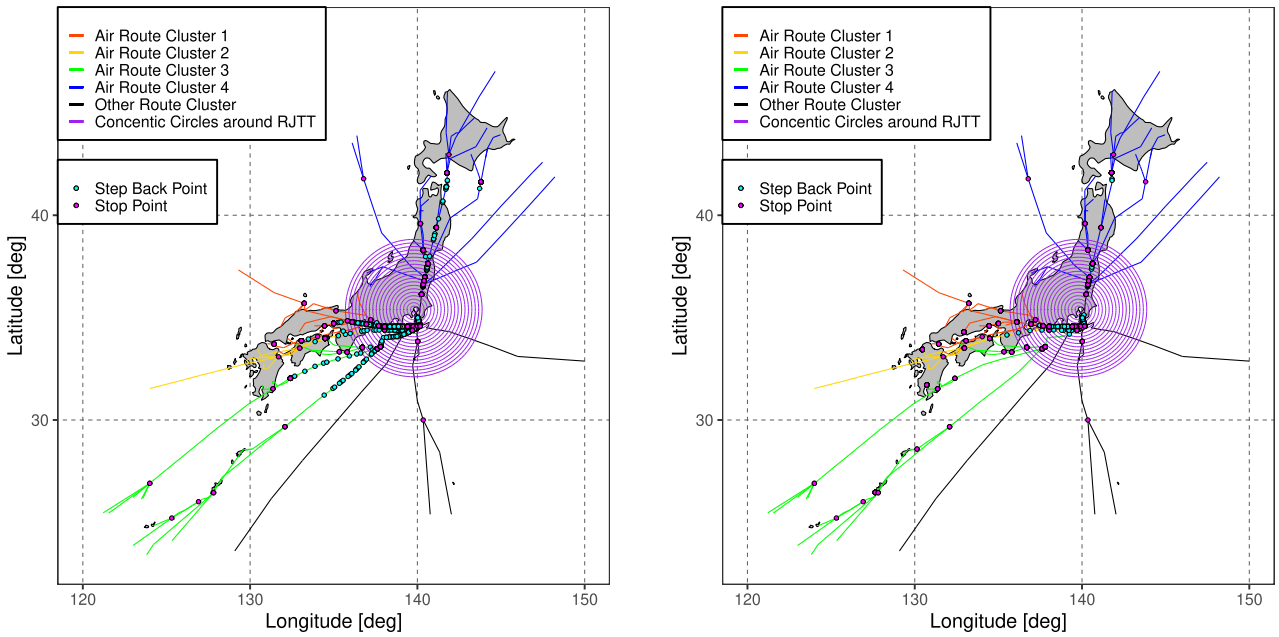

(a) Original solution

(b) Minimum fuel solution

FIGURE 10. Mapping of spacing adjustments.

flights, respectively. The blue and red lines indicate the flights landing at runway 34R and 34L, respectively. The arrival delay values of several flights in the original solution were greater than 5 min, as shown in Fig. 9(a). In addition, a few flights reported arrival delays in excess of 10 min at both 34L and 34R. However, the arrival delays of several flights were drastically reduced in the minimum fuel solution, as shown in Fig. 9(b). In particular, the minimum fuel solution successfully reduced the arrival delays of several flights landing on runway 34L. In addition, the arrival delays of several flights landing at 34L were reduced to less than 5 min. Some of the flights even touched down approximately 5 min before the flights on the original schedule. Hence, we can state that the minute takeoff time adjustments made in the minimum fuel solution contributed to relieving traffic congestion.

Several factors contribute to the simultaneous reduction of arrival delay and fuel consumption. An additional analysis demonstrated that the reduction of these parameters coincided with the reduction of conflicts in the en-route airspace. Therefore, Section V-C analyzes the impact of spacing adjustments, such as the "Step Back" and "Stop" CA rules.

C. ANALYZING SPACING ADJUSTMENT

Table 5 lists the number of spacing adjustments, such as the "Step Back" and "Stop" movements, made in each solution.

TABLE 5. Total number of the spacing adjustments.

Movement	Original Solution	Minimum Fuel Solution
Step Back	2687	544
Stop	28238	5564

The total number of "Step Back" and "Stop" movements in the minimum fuel solution are significantly less than those in the original solution, as presented in Table 5. The total number of "Step Back" and "Stop" movements in the original solution are 2687 and 28238, respectively. These values are reduced by approximately 80 % in the minimum fuel solution. The minor takeoff time adjustments for each flight drastically decreased the number of conflicts in the en-route air space. Therefore, the arrival delay and fuel consumption were successfully reduced, as mentioned in Section V-B.

Figure 10 depicts the points of implementation of the spacing adjustments according to the CA rules. Air routes leading to RJTT are divided into four representative groups according to their origin points. Table 6 summarize the characteristics of each air route cluster depicted in Fig. 10. Although only 598 flights have been mentioned in Table 6, the other 9 international flights fly on the other route cluster depicted as black lines in Fig. 10 with few interactions. Air route clusters 1, 2, and 3 include the traffic arriving at RJTT from the southwestern direction, whereas air route cluster 4 includes the traffic coming from the northern direction. Air route cluster 1 includes short-haul flights, while air route clusters 2 and 3 are predominantly composed of long-haul flights. Air route

TABLE 6. Total number of flights in each air route cluster.

Cluster	# of flights	Main Flights	Direction
1	192	Short-haul	Southwest
2	114	Long-haul	Southwest
3	152	Long-haul&Short-haul	Southwest
4	140	Long-haul&Short-haul	North

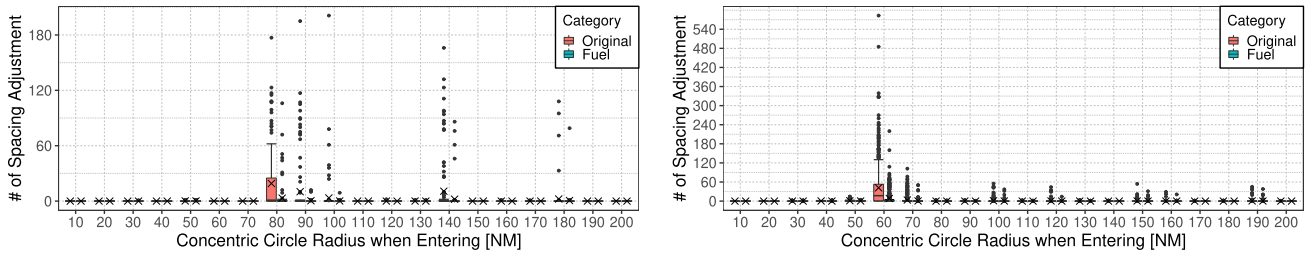

(a) North traffic

(b) South traffic

FIGURE 11. Number of spacing adjustments for different radii of entry.

cluster 3 had more pop-up flights than air route cluster 2. The blue and red circles represent the geographical points where the ''Step Back'' and ''Stop'' rules were applied, respectively. The concentric purple circles are plotted after every 10 NM within a radius of 200 NM. The ''Step Back'' movement is implemented across the area close to RJTT, while the ''Stop'' movement is conducted primarily at the confluence points, as shown in Fig. 10(a). These spacing adjustments are largely implemented in the region between longitudes of 130° E and 140° E and latitudes of 30° N and 35° N. However, the number of the spacing adjustments implemented in the minimum fuel solution is significantly less than that in the original solution, as shown in Fig. 10(b). Specifically, the number of geographical points representing the application of the ''Step Back'' in the area between the 40 NM and 200 NM radii in the southwestern direction is reduced in the minimum fuel solution. Further, the number of ''Step Back'' adjustments made in the region between the 100 NM and 200 NM radii on air route clusters 1 and 2 was significantly reduced in the minimum fuel solution. Similarly, the number of ''Step Back'' adjustments made in the region beyond the 200 NM radius on air route clusters 3 and 4 was less in the minimum fuel solution than that in the original solution. In addition, the geographical points of application of the ''Step Back'' rule were absent in the regions beyond the 100 NM radius on air route cluster 3. Several pop-up flights merged on this route cluster. Thus, the conflicts in the en-route airspace are substantially reduced due to the minute takeoff time differences, as shown in Fig 14. Notably, the number of spacing adjustments in the minimum fuel solution is reduced not only in the en-route airspace but also in the terminal airspace enclosed within the 100 NM radius centered at RJTT.

Figure 11 depicts the number of spacing adjustments made after 10 NM radius segments. The horizontal axis represents the radius of entry for the aircraft, and the vertical axis represents the number of spacing adjustments. The flights coming from the northern and southwestern directions are independent of each other because their routes are separated. Hence, Fig. 11(a) includes the flights arriving from the northern direction, whereas Fig. 11(b) includes the flights arriving from the southwestern direction. There are significant differences among the number of spacing adjustments made in the original solution in the regions enclosed between the 70 NM and 100 NM radii, the 130 NM and 140 NM radii, and the 170 NM and 180 NM radii in the northern direction. The maximum mean number of spacing adjustments is approximately 30. These adjustments occur in the region between the 70 NM and 80 NM radii, which corresponds to the last merging point before arrival. However, the variation among the number of spacing adjustments made in these areas is considerably reduced in the minimum fuel solution. The mean number of spacing adjustments is significantly reduced as well. These areas correspond to the confluence points and surroundings in the northern direction, as shown in Fig. 10. Similarly, the variation of the number of spacing adjustments in the area between the 50 NM and 70 NM radii in the southwestern direction is significantly less in the minimum fuel solution than that of the original solution, as shown in Fig. 11(b). The maximum mean number of spacing adjustments in the airspace between the 50 NM and 60 NM radii is approximately equal to 60, which corresponds to the last merging point before arrival. The maximum mean and variance in the airspace between the 50 NM and 60 NM radii in the southwestern direction are significantly greater than the corresponding values in the airspace between the 70 NM and 80 NM radii. Therefore, we can state that the reduction in the number of spacing adjustments around the confluence points that are located before the terminal maneuvering area reduces both the arrival delay and fuel consumption.

The most remarkable result to emerge from the data comparison is the significant reduction in the number of spacing adjustments in the terminal airspace. Terminal airspaces witness a large number of spacing adjustments because of the simultaneous arrival of the inbound traffic at RJTT, as shown in Fig. 11(a). According to the specified CA parameters d and BD, these flights attempt to maintain a sufficient in-trial separation when they come close to each other. Feasible solutions to avoid conflicts can be automatically generated by using the evolutionary algorithm. In particular, the ''Step Back'' movement would have a more negative impact than the ''Stop'' movement because the former would reduce the space between the proceeding and succeeding flights. Hence, the number of ''Step Back'' movements in the en-route space are reduced, as depicted in Fig 10. These results indicate that the operation wherein the flights takeoff in order to maintain sufficient separation in the terminal airspace significantly reduces the arrival delay and fuel consumption as a result of the reduced conflicts. In reality, there are many

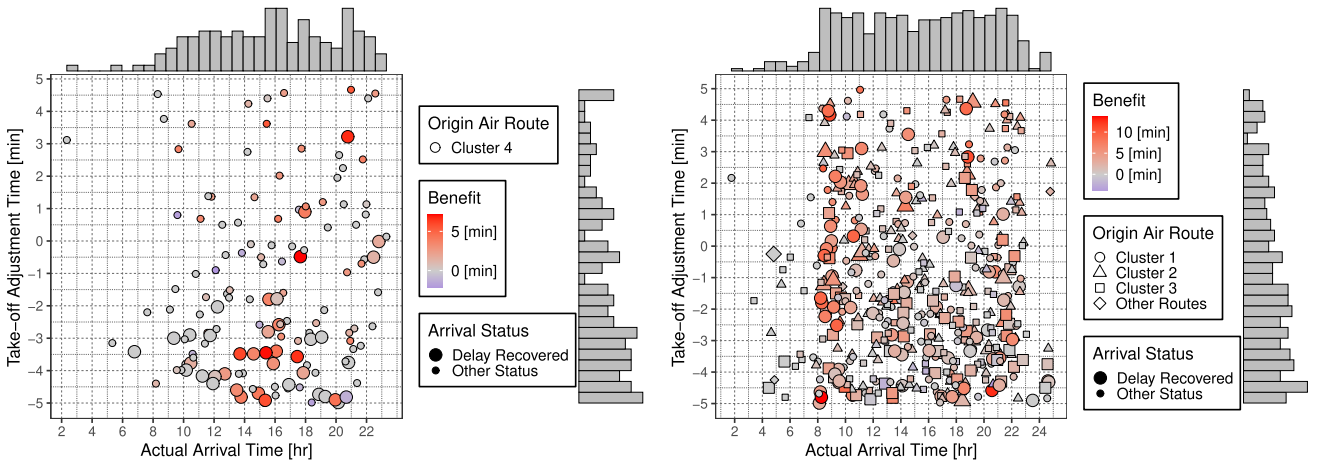

(a) Northern inbound traffic

(b) Southwestern inbound traffic

FIGURE 12. Sscatter plot of the design variable.

flights excluding the arrival flights for RJTT. However, this study focuses to adjust the takeoff time at the level of delay, which gets overlapped with the in-flight phase. Therefore, the airspace demand in the en-route sectors would not change drastically. In this situation, air traffic controllers in those sectors could safely provide directions to the pilots to avoid any conflicts in the flight travels. Additional analyses are conducted in Section V-D to clarify the possibility of implementing this operation.

D. ANALYZING DESIGN VARIABLES AND THE TAKEOFF TIME

Figure 12 shows the scatter plot of the design variable. The horizontal axis represents the actual arrival time obtained in the minimum fuel solution. The vertical axis represents the value of the design variable. The marginal distributions are additionally depicted according to each axis. The design variables are allotted different shapes according to the air route clusters. The symbols representing the flights whose delays have been recovered have larger sizes than those representing other statuses. Flights arriving 5 min after the scheduled arrival time are classified as delayed flights. Benefit refers to the quantitative benefit of the design variables. $Benefit(i)$ $(i = 1, 2, \cdots, 607)$ is calculated as follows:

$$Benefit(i) = Delay_{org}(i) - Delay_{fuel}(i) + Var(i) \qquad (2)$$

where i denotes the number allocated to a flight. Further, $Delay_{org}(i)$ represents the arrival delay reported in the original schedule, and $Delay_{fuel}(i)$ represents the arrival delay reported in the minimum fuel solution. $Var(i)$ is the takeoff adjustment time for each flight. A large benefit indicates that the takeoff time adjustment of the flight is more efficient than that of a flight with a small benefit. As the benefit values of almost all flights are greater than 0, as shown in Fig. 12, it can be stated that the takeoff time adjustments are successfully implemented in general. The red-colored design variables, which represent high benefit values, were clustered between 13 and 18 hours for traffic inbound from the northern direction, as shown in Fig. 12(a). However, the traffic inbound from the southwestern direction reported high benefit design variables between 8 and 11 hours and 17 and 22 hours. Flights with such design variables arrive during congested hours because the number of arrivals during these hours is higher than it is during other hours according to the marginal distribution of the actual arrival time. Further, most flights with high benefits have recovered time delays status and are depicted by the symbols having a larger size than the rest, as shown in Fig 12. The number of flights having a takeoff time earlier than that mentioned in the original schedule is slightly higher than the number of flights having a delayed takeoff, as shown in the marginal distribution of the takeoff adjustment time. Notably, some flights arriving during congested hours recovered from their delayed statuses by delaying their takeoff time. Further, the flights whose delays are recovered during the morning hours generally belong to air route cluster 1 and are represented by a circle in Fig 12(b). This is because the number of flights belonging to air route cluster 1 is higher than that of the other air route clusters, as shown in Table 6.

The above results indicate that controlling the takeoff time during congested hours would be highly effective, as shown in Fig. 12. Several perspectives could be considered to adjust the takeoff time appropriately. We further studied two perspectives, namely, the takeoff time difference at the same origin and the time interval at specific fixes that are close to the entry points of the terminal airspace. According to the perspective of the takeoff time difference at the same origin, the number of flights departing from the same origin to RJTT tends to increase within a few minutes due to the high demand during congested hours. Therefore, the takeoff time interval at such origins is likely to be less than that of other low-demand origins. However, this narrow interval could negatively impact the in-trail separation in the terminal region. In addition, pop-up flights could disturb the

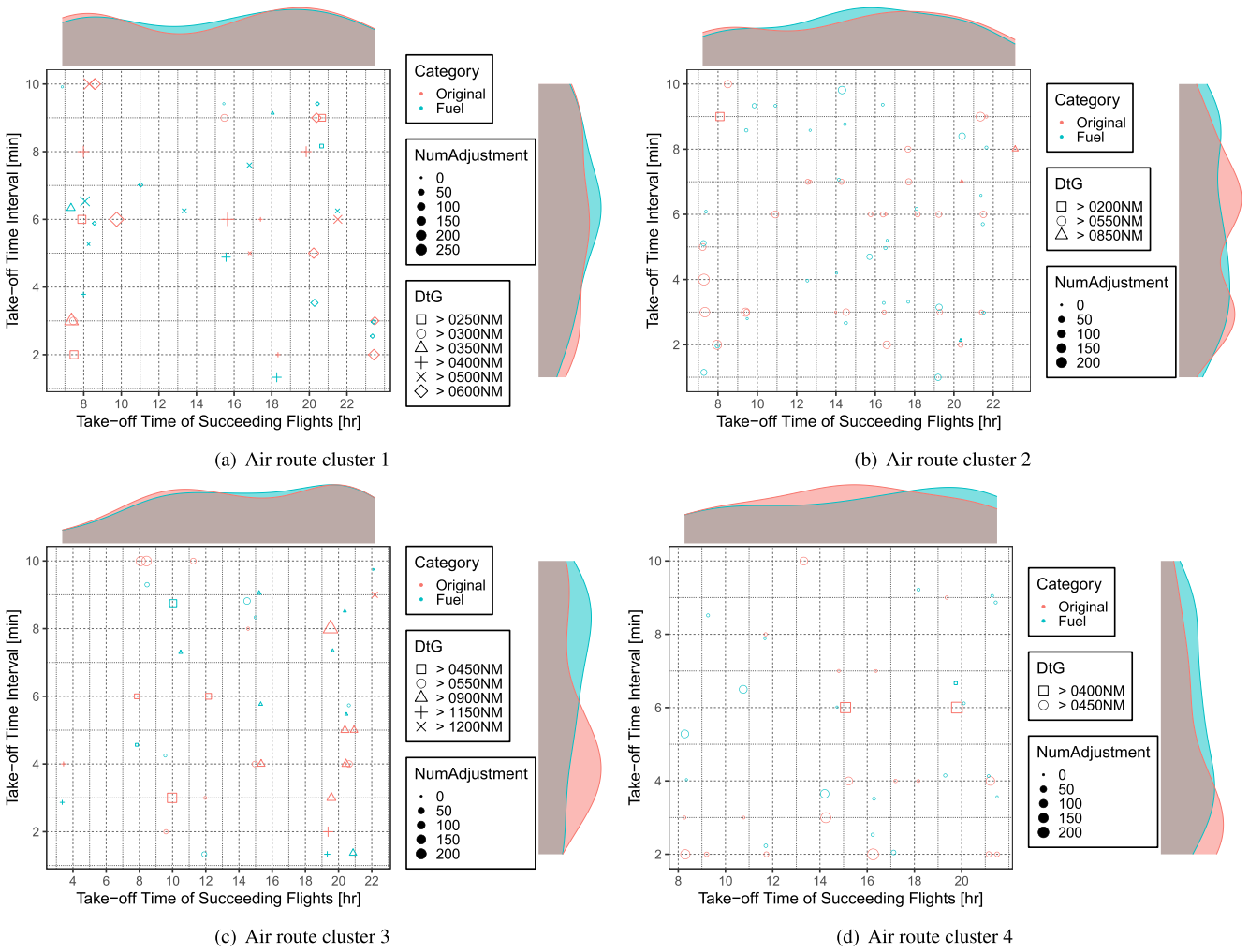

FIGURE 13. Scatter plot of the takeoff time interval at the same origin.

tailored separation. Thus, according to the current perspective, the time interval at the point of merging of the pop-up flights is important.

Figure 13 depicts the scatter plot of the takeoff time interval at the same origin. The horizontal axis represents the takeoff time of successive flights at the same origin. The vertical axis represents the takeoff time interval between the proceeding and succeeding flights at the same origin. The marginal density distributions are additionally depicted for each axis.

The flights obtained from the original solution and the minimum fuel solution are represented by red and blue symbols, respectively. The size of the symbol corresponds to the number of spacing adjustments. In addition, the shape of the symbol varies according to the distance of the flight to RJTT (e.g., "$>$0200 NM" indicates that the distance to RJTT is greater than 200 NM and less than 300 NM). The number of spacing adjustments in the original solution increased significantly during the morning and evening hours in air route clusters 1–3, while it increased during the afternoon in air cluster route 4. This corresponds to a congested time when the benefit depicted in Fig 12 is remarkably high. In contrast, the number of spacing adjustments in the minimum fuel solution depicts a reduction during these congested hours. In addition, the marginal density distribution of the original solution is higher than that of the minimum fuel solution during these hours. This indicates that the minimum fuel solution reduces the number of flights that have a takeoff time interval greater than 10 min. However, the marginal density distribution of the original solution during non-congested hours is lower than that of the minimum fuel solution. Hence, the minimum fuel solution adjusts the takeoff time such that the interval is as long as possible during congested time and as short as possible during non-congested hours. The peak of the density distribution of the takeoff time interval is relatively higher in the minimum fuel solution, as shown in the marginal density distribution of the takeoff time interval. The peak of the marginal density distribution of the takeoff time interval in the original solution was approximately 4 min, whereas the peal of the minimum fuel solution was greater than 4 min. Therefore, the takeoff time interval of flights traveling to the same destination from the same origin should be relatively higher.

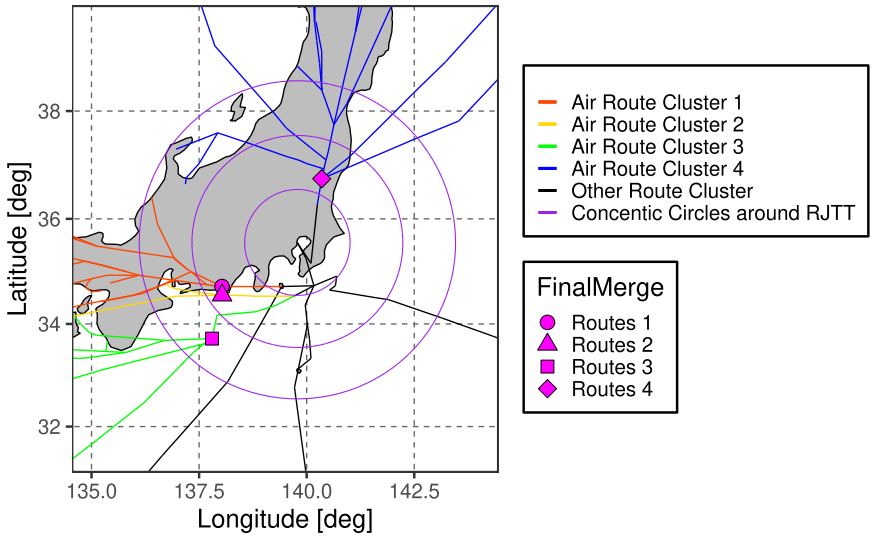

FIGURE 14. Air route and final merging point around RJTT.

TABLE 7. Summary of the time interval at 7 NM before the final confluence point of each air route cluster.

Cluster	Mean$_{org}$ [sec]	Mean$_{fuel}$ [sec]	Difference of Mean [sec]	SD$_{org}$ [sec]	SD$_{fuel}$ [sec]	Difference of SD [sec]
1	221.1	238.0	+16.9	156.9	138.1	−18.8
2	251.8	269.4	+17.6	147.5	153.5	+6.0
3	256.5	239.2	−17.3	183.8	146.9	−36.9
4	200.2	224.9	+24.7	124.2	105.3	−18.9

Figure 15 and Table 7 depict the histogram and the summary of the time interval before the final merge point of each air route cluster that is depicted in Fig. 14. The concentric purple circles are plotted after 60 NM within a radius of 180 NM. The results of air route clusters 1, 2, and 3 are discussed separately from that of air route cluster 4 because the parameters of the model, namely, d and BD, are different, as shown in Table 3. The mean time interval of the final merge point of air route cluster 1 increased by 16.9 s, and its standard deviation decreased by 18.8 s. The frequency of the time interval of the original solution, which is depicted in red, is higher than that of the minimum fuel solution, which is depicted in blue, at approximately 1 min, as shown in Fig. 15(a). In contrast, the frequency of the minimum fuel solution at approximately 3 min is higher than that of the original solution. Therefore, more succeeding flights are sufficiently separated from proceeding flights at the final merge point of air route cluster 1. Similarly, the mean time interval of the final merge point of air route cluster 2 increases by 17.6 s, as shown in Table 7. The time interval of this cluster was greater than air route clusters 1 and 2 because the number of flights in this cluster was the lowest in air route clusters 1, 2, and 3. Therefore, the mean time interval of air route cluster 2 obtained from the minimum fuel solution is greater than those of air route clusters 1 and 3. In contrast, the mean and standard deviation of the time interval of air route cluster 3 before the final merge point reduced drastically declined. It is noteworthy that several pop-up and long-haul flights merge at the final merge point in air route cluster 3. The standard deviation of the time interval in air route cluster 3 obtained from the original solution is greater than the other clusters, as shown in Table 7. However, this variation is suppressed in the minimum fuel solution. Consequently, the values of the resulting mean and standard deviation of the time interval are similar to the values of air route cluster 1. The mean time interval of air route cluster 4 increases by 24.7 s, while its standard deviation reduces by 18.9 s. The absolute values of the mean and standard deviation of air route cluster 4 are greater than those of air route clusters 1, 2, and 3 because the parameters of the model, namely d and BD, are greater for air route cluster 4 than they are for the other air route clusters. In addition, the distribution of the time interval of air route cluster 4 is similar to a normal distribution because the final merge point of air route cluster 4 is identical to the final merge point of the traffic coming from the northern direction, as depicted in Fig. 15(d). The peak of the distribution increases, and its variance decreases, as shown in Table 7.

Barring a few exceptions, these results demonstrate that the time interval at the final merge point that is close to the terminal increases with minimal variation in the minimum fuel solution, as shown in Fig 15 and Table 7. This result implies that the spacing adjustments can be reduced by not only maintaining a sufficient in-trial separation while also minimizing the deviation of this time interval.

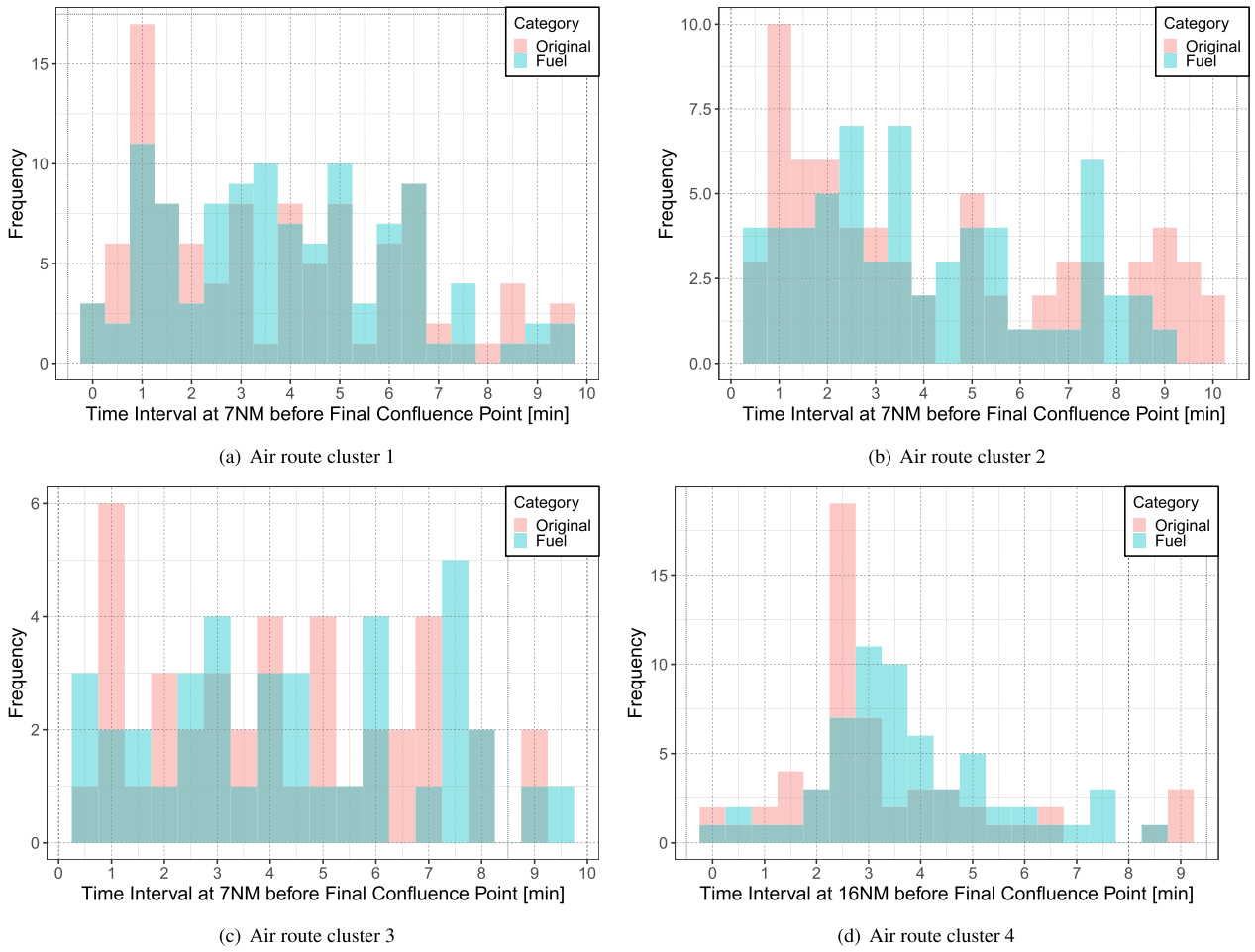

(a) Air route cluster 1

(b) Air route cluster 2

(c) Air route cluster 3

(d) Air route cluster 4

FIGURE 15. Histogram of the time interval before the final confluence point of each air route cluster.

VI. CONCLUSION

We conducted the multi-objective air traffic optimization of schedule design by using a step-back cellular automaton in this study. The objective functions were to minimize (1) the total arrival delay and (2) total fuel consumption. The design variable used in the study was the time difference between the scheduled and actual takeoff time within ±300 s. The number of the design variables was equal to 607 and included both domestic and international flights landing at Tokyo International Airport (RJTT).

The results of the multi-objective optimization produced several non-dominated solutions that were superior to the solution corresponding to the original schedule. The total arrival delay and total fuel consumption were reduced by approximately 1500 min and 80 tons, respectively. This study highlights the importance of making minor adjustments in the takeoff time. The analyses of the objective function and design variable indicate that both objective functions can be minimized simultaneously by performing takeoff time adjustments in an identical manner.

Detailed comparisons between the original solution and the minimum fuel solution presented two significant findings. Minor takeoff adjustments contribute to a significant reduction in the number of spacing adjustments. These adjustments lead to the reduction of arrival delay and fuel consumption. Further, the takeoff time adjustment is highly effective during periods of high traffic demand in the terminal space. The quantitative benefit provided to several flights is expected to be more than 5 min during the congested time periods.

Two effective operations can be proposed on the basis of the current findings and additional analyses. The takeoff time interval of flights originating from the same point during congestion hours should be longer than those during non-congestion hours. Pop-up flights should merge with sufficient in-trail separation and minimum variation of the time interval. Therefore, we can conclude that the optimization of airport operations, such as takeoff time, spot assignment, and taxi routes, has a significant impact on air traffic flow. Although this paper focuses on traffic arriving at RJTT on a specific date, the proposed approach is applicable for any type of traffic on different dates because NSGA-II is a meta-heuristic optimization method, which has the potential to provide sufficient solutions to the problem of takeoff time adjustments for each flight.

In the future, we intend to conduct optimization studies considering various scenarios, such as runway changes and inclement weather, to provide an ATM with sufficient resilience. We hope that it will eventually be possible to improve the SBCA model to consider flights excluding arrival traffic at RJTT.

ACKNOWLEDGMENT

The authors would like to thank the Ministry of Land, Infrastructure, Transport and Tourism (MLIT) for providing access to the CARATS Open Data. The authors would also like to thank the Electronic Navigation Research Institute for supplying the information that was crucial in developing the route and timetable for the simulations.

REFERENCES

[1] *ICAO Long-Term Traffic Forecasts Passenger and Cargo*, Int. Civil Aviation Org., Montreal, QC, Canada, 2016.
[2] *Five Years to Return to the PrePpandemic Level of Passenger Demand*, Int. Air Transp. Assoc., Montreal, QC, Canada, 2019.
[3] *Global Air Traffic Management Operational Concept*, Int. Civil Aviation Org., Montreal, QC, Canada, 2005.
[4] *Concept of Operations for the Next Generation Air Transportation System Ver. 3.2*, Federal Aviation Admin. Joint Planning Develop., Washington, DC, USA, 2010.
[5] *European ATM Master Plan Edition 2015*, ESAR Joint Undertaking, Brussels, Belgium, 2015.
[6] *Long-Term Vision for the Future Air Traffic Systems*, Jpn. Civil Aviation Bur., Tokyo, Japan, 2010.
[7] A. R. Odoni, "The flow management problem in air traffic control," in *Flow Control of Congested Networks*. (NATO ASI Series: Series F: Computer and Systems Sciences), vol. 38. Berlin, Germany: Springer, 1987, doi: 10.1007/978-3-642-86726-2_17.
[8] M. Terrab and A. R. Odoni, "Strategic flow management for air traffic control," *Oper. Res.*, vol. 41, no. 1, pp. 138–152, Feb. 1993.
[9] O. Richetta and A. R. Odoni, "Solving optimally the static ground-holding policy problem in air traffic control," *Transp. Sci.*, vol. 27, no. 3, pp. 228–238, Aug. 1993.
[10] O. Richetta and A. R. Odoni, "Dynamic solution to the ground-holding problem in air traffic control," *Transp. Res. A, Policy Pract.*, vol. 28, no. 3, pp. 167–185, May 1994.
[11] M. O. Ball, R. Hoffman, A. R. Odoni, and R. Rifkin, "A stochastic integer program with dual network structure and its application to the ground-holding problem," *Oper. Res.*, vol. 51, no. 1, pp. 167–171, Feb. 2003.
[12] A. Mukherjee and M. Hansen, "A dynamic stochastic model for the single airport ground holding problem," *Transp. Sci.*, vol. 41, no. 4, pp. 444–456, Nov. 2007.
[13] Y. Liu and M. Hansen, "Incorporating predictability into cost optimization for ground delay programs," *Transp. Sci.*, vol. 50, no. 1, pp. 132–149, Feb. 2016.
[14] Y. Wang and D. Kulkarni, "Modeling weather impact on ground delay programs," *SAE Int. J. Aerosp.*, vol. 4, no. 2, pp. 1207–1215, Oct. 2011.
[15] A. Mukherjee, S. Grabbe, and B. Sridhar, "Predicting ground delay program at an airport based on meteorological conditions," in *Proc. 14th AIAA Aviation Technol., Integr., Oper. Conf.*, 2014, pp. 2713–2718.
[16] M. Bloem and N. Bambos, "Ground delay program analytics with behavioral cloning and inverse reinforcement learning," *J. Aerosp. Inf. Syst.*, vol. 12, no. 3, pp. 299–313, Mar. 2015.
[17] K. D. Kuhn, "A methodology for identifying similar days in air traffic flow management initiative planning," *Transp. Res. C, Emerg. Technol.*, vol. 69, pp. 1–15, Aug. 2016.
[18] Y. Xu, S. Wandelt, and X. Sun, "Robust integrated airline scheduling with chance constraints," in *Proc. 9th Int. Conf. Res. Air Transp. (ICRAT)*, 2020. [Online]. Available: http://www.icrat.org/icrat/
[19] L. K. Hassan, B. F. Santos, and J. Vink, "Airline disruption management: A literature review and practical challenges," *Comput. Oper. Res.*, vol. 127, Mar. 2021, Art. no. 105137.
[20] H. D. Sherali, K.-H. Bae, and M. Haouari, "Integrated airline schedule design and fleet assignment: Polyhedral analysis and benders' decomposition approach," *Informs J. Comput.*, vol. 22, no. 4, pp. 500–513, Nov. 2010.
[21] H. Jiang and C. Barnhart, "Robust airline schedule design in a dynamic scheduling environment," *Comput. Oper. Res.*, vol. 40, no. 3, pp. 831–840, Mar. 2013.
[22] J. P. Pita, N. Adler, and A. P. Antunes, "Socially-oriented flight scheduling and fleet assignment model with an application to Norway," *Transp. Res. B, Methodol.*, vol. 61, pp. 17–32, Mar. 2014.
[23] L. Cadarso and R. de Celis, "Integrated airline planning: Robust update of scheduling and fleet balancing under demand uncertainty," *Transp. Res. C, Emerg. Technol.*, vol. 81, pp. 227–245, Aug. 2017.
[24] O. Faust, J. Gönsch, and R. Klein, "Demand-oriented integrated scheduling for point-to-point airlines," *Transp. Sci.*, vol. 51, no. 1, pp. 196–213, Feb. 2017.
[25] N. Kenan, A. Jebali, and A. Diabat, "The integrated aircraft routing problem with optional flights and delay considerations," *Transp. Res. E, Logistics Transp. Rev.*, vol. 118, pp. 355–375, Oct. 2018.
[26] K. Wei, V. Vaze, and A. Jacquillat, "Airline timetable development and fleet assignment incorporating passenger choice," *Transp. Sci.*, vol. 54, no. 1, pp. 139–163, Dec. 2019.
[27] L. H. Lee, C. U. Lee, and Y. P. Tan, "A multi-objective genetic algorithm for robust flight scheduling using simulation," *Eur. J. Oper. Res.*, vol. 177, no. 3, pp. 1948–1968, Mar. 2007.
[28] K. K. H. Ng, C. K. M. Lee, F. T. S. Chan, and Y. Lv, "Review on meta-heuristics approaches for airside operation research," *Appl. Soft Comput.*, vol. 66, pp. 104–133, May 2018.
[29] A. Pellegrini, P. D. Sanzo, B. Bevilacqua, G. Duca, D. Pascarella, R. Palumbo, J. J. Ramos, M. A. Piera, and G. Gigante, "Simulation-based evolutionary optimization of air traffic management," *IEEE Access*, vol. 8, pp. 161551–161570, 2020.
[30] G. Froyland, S. J. Maher, and C.-L. Wu, "The recoverable robust tail assignment problem," *Transp. Sci.*, vol. 48, no. 3, pp. 351–372, Aug. 2014.
[31] Z. Liang, F. Xiao, X. Qian, L. Zhou, X. Jin, X. Lu, and S. Karichery, "A column generation-based heuristic for aircraft recovery problem with airport capacity constraints and maintenance flexibility," *Transp. Res. B, Methodol.*, vol. 113, pp. 70–90, Jul. 2018.
[32] M. Zanin, Y. Zhu, R. Yan, P. Dong, X. Sun, and S. Wandelt, "Characterization and prediction of air transport delays in China," *Appl. Sci.*, vol. 10, no. 18, p. 6165, Sep. 2020.
[33] K. Deb, A. Pratap, S. Agarwal, and T. Meyarivan, "A fast and elitist multiobjective genetic algorithm: NSGA-II," *IEEE Trans. Evol. Comput.*, vol. 6, no. 2, pp. 182–197, Apr. 2002.
[34] R. M. Harris, "Models for runway capacity analysis," MITRE Corp., Langley, VA, USA, Tech. Rep. MTR-4102, Rev. 2, 1972.
[35] M. Janić and V. Tošić, "Terminal airspace capacity model," *Transp. Res. A, Gen.*, vol. 16, no. 4, pp. 253–260, Jul. 1982.
[36] M. Hansen, "Micro-level analysis of airport delay externalities using deterministic queuing models: A case study," *J. Air Transp. Manage.*, vol. 8, no. 2, pp. 73–87, Mar. 2002.
[37] N. Pyrgiotis, K. M. Malone, and A. Odoni, "Modelling delay propagation within an airport network," *Transp. Res. C, Emerg. Technol.*, vol. 27, pp. 60–75, Feb. 2013.
[38] P. K. Menon, G. D. Sweriduk, and K. D. Bilimoria, "New approach for modeling, analysis, and control of air traffic flow," *J. Guid., Control, Dyn.*, vol. 27, no. 5, pp. 737–744, Sep. 2004.
[39] P. K. Menon, G. D. Sweriduk, T. Lam, G. M. Diaz, and K. D. Bilimoria, "Computer-aided eulerian air traffic flow modeling and predictive control," *J. Guid., Control, Dyn.*, vol. 29, no. 1, pp. 12–19, Jan. 2006.
[40] D. B. Work and A. M. Bayen, "Convex formulations of air traffic flow optimization problems," *Proc. IEEE*, vol. 96, no. 12, pp. 2096–2112, Dec. 2008.
[41] D. Sun and A. M. Bayen, "Multicommodity eulerian-lagrangian large-capacity cell transmission model for en route traffic," *J. Guid., Control, Dyn.*, vol. 31, no. 3, pp. 616–628, May 2008.
[42] P. Wei, Y. Cao, and D. Sun, "Total unimodularity and decomposition method for large-scale air traffic cell transmission model," *Transp. Res. B, Methodol.*, vol. 53, pp. 1–16, Jul. 2013.
[43] H. Zhang, Y. Xu, L. Yang, and H. Liu, "Macroscopic model and simulation analysis of air traffic flow in airport terminal area," *Discrete Dyn. Nature Soc.*, vol. 2014, pp. 1–15, Aug. 2014.
[44] T. Ezaki and K. Nishinari, "Potential global jamming transition in aviation networks," *Phys. Rev. E, Stat. Phys. Plasmas Fluids Relat. Interdiscip. Top.*, vol. 90, no. 2, Aug. 2014, Art. no. 022807.
[45] D. Chen, M. Hu, Y. Ma, and J. Yin, "A network-based dynamic air traffic flow model for short-term en route traffic prediction," *J. Adv. Transp.*, vol. 50, no. 8, pp. 2174–2192, Dec. 2016.
[46] K. K. H. Ng, C. K. M. Lee, F. T. S. Chan, C.-H. Chen, and Y. Qin, "A two-stage robust optimisation for terminal traffic flow problem," *Appl. Soft Comput.*, vol. 89, Apr. 2020, Art. no. 106048.

[47] K. K. H. Ng, C.-H. Chen, and C. K. M. Lee, "Mathematical programming formulations for robust airside terminal traffic flow optimisation problem," *Comput. Ind. Eng.*, vol. 154, Apr. 2021, Art. no. 107119.
[48] S. Alam, H. A. Abbass, and M. Barlow, "ATOMS: Air traffic operations and management simulator," *IEEE Trans. Intell. Transp. Syst.*, vol. 9, no. 2, pp. 209–225, Jun. 2008.
[49] D. Šišlák, P. Volf, and M. Pěchouček, "Agent-based cooperative decentralized airplane-collision avoidance," *IEEE Trans. Intell. Transp. Syst.*, vol. 12, no. 1, pp. 36–46, Mar. 2011.
[50] A. K. Agogino and K. Tumer, "A multiagent approach to managing air traffic flow," *Auto. Agents Multi-Agent Syst.*, vol. 24, no. 1, pp. 1–25, Jan. 2012.
[51] Y. Guleria, Q. Cai, S. Alam, and L. Li, "A multi-agent approach for reactionary delay prediction of flights," *IEEE Access*, vol. 7, pp. 181565–181579, 2019.
[52] D. Sun, I. S. Strub, and A. M. Bayen, "Comparison of the performance of four eulerian network flow models for strategic air traffic management," *Netw. Heterogeneous Media*, vol. 2, no. 4, p. 569, 2007.
[53] P. Sarkar, "A brief history of cellular automata," *ACM Comput. Surv.*, vol. 32, no. 1, pp. 80–107, Mar. 2000.
[54] C. Kim, K. Abubaker, and O. Obah, "Cellular automata modeling of en route and arrival self-spacing for autonomous aircrafts," in *Proc. 50th Annu. Meeting Air Traffic Controllers Assoc.*, 2005, pp. 127–134.
[55] S.-P. Yu, X.-B. Cao, and J. Zhang, "A real-time schedule method for aircraft landing scheduling problem based on cellular automation," *Appl. Soft Comput.*, vol. 11, no. 4, pp. 3485–3493, Jun. 2011.
[56] Y. He, K. Cai, Y. Li, and M. Xiao, "An improved Cellular-Automaton-Based algorithm for real-time aircraft landing scheduling," in *Proc. 7th Int. Symp. Comput. Intell. Design*, vol. 1, Dec. 2014, pp. 284–288.
[57] S.-J. Wang and Y.-H. Gong, "Research on air route network nodes optimization with avoiding the three areas," *Saf. Sci.*, vol. 66, pp. 9–18, Jul. 2014.
[58] W.-X. Lim and Z.-W. Zhong, "Re-planning of flight routes avoiding convective weather and the 'three areas,'" *IEEE Trans. Intell. Transp. Syst.*, vol. 19, no. 3, pp. 868–877, Mar. 2018.
[59] F. Enayatollahi and M. A. A. Atashgah, "Wind effect analysis on air traffic congestion in terminal area via cellular automata," *Aviation*, vol. 22, no. 3, pp. 102–114, Nov. 2018.
[60] F. Enayatollahi, M. A. A. Atashgah, S. M. Malaek, and P. Thulasiraman, "PBN-based time-optimal terminal air traffic control using cellular automata," *IEEE Trans. Aerosp. Electron. Syst.*, early access, Jan. 21, 2021, 10.1109/TAES.2020.3048787.
[61] T. Tatsukawa, S. Nagaoka, K. Anzai, and K. Fujii, "A study of air traffic simulation around haneda airport using step back cellular automaton," in *Proc. AIAA Guid., Navigat., Control Conf.*, Jan. 2018, p. 1597.
[62] K. Sekine, T. Tatsukawa, S. Nagaoka, and K. Fujii, "Preliminary study of multi-objective air traffic optimization by using step back cellular automaton," in *Proc. AIAA Aviation Forum*, Jun. 2019, p. 3407.
[63] EUROCONTROL. (2015). *Base of Aircraft Data (BADA)*. [Online]. Available: https://www.eurocontrol.int/sites/default/files/publication/files/bada-factsheet.pdf
[64] *Passenger Traffic 2017 Final (Annual)*, Airports Council Int., Brussels, Belgium, 2019.
[65] (2015). *Air Navigation Services Department Civil Aviation Bureau, MLIT*. Data Extracted From the Air Navigation Services Department's Database Becomes. [Online]. Available: https://www.mlit.go.jp/common/001082594.pdf

KATSUHIRO SEKINE received the B.S. degree in industrial management and engineering from the Tokyo University of Science, Tokyo, Japan, in 2019, where he is currently pursuing the master's degree.

He visited the German Aerospace Center (DLR) as a Research Trainee during his career and carried out research on extended arrival management. He is also a Research Trainee at the Air Traffic Management Department, Electronic Navigation Research Institute (ENRI), and the National Institute of Maritime, Port and Aviation Technology. His research interests include multi-objective optimization, statistical and machine learning method, modeling and simulation, and their applications in air traffic management.

TOMOAKI TATSUKAWA (Member, IEEE) received the B.S. and M.S. degrees in engineering from the Tokyo Institute of Technology, Tokyo, Japan, in 2002 and 2004, respectively, and the Ph.D. degree in engineering from The University of Tokyo, Tokyo, in 2012.

He was a Software Engineer at SGI Japan Ltd., from 2004 to 2010. From 2012 to 2015, he was a Postdoctoral Research Fellow with the Institute of Space and Astronautical Science, Japan Aerospace Exploration Agency (ISAS/JAXA), Sagamihara, Japan. From 2015 to 2019, he was a Junior Associate Professor at the Tokyo University of Science, Tokyo. Since April 2020, he has been an Associate Professor with the Department of Information and Computer Technology, Tokyo University of Science. His research interests include multi-objective evolutionary computation, aerodynamic design optimization, and multi-objective design exploration. He is a member of the JSME. He received the Young Researcher Award from the IEEE Computational Intelligence Society Japan Chapter, in 2011.

ERI ITOH received the Ph.D. degree in aeronautics and astronautics from The University of Tokyo, Japan, in 2017.

After her research experience at the Euroconctol Experimental Centre, the Netherlands Aerospace Centre: NLR, the NASA's Ames Research Center, and the Nanyang Technological University, she currently holds positions as an Associate Professor at the Aeronautics and Astronautics Department, The University of Tokyo, and also a Chief Researcher at the Air Traffic Management Department, Electronic Navigation Research Institute, and the National Institute of Maritime, Port and Aviation Technology. Her research interests include automation system design, which collaborates with human operators, the air traffic management, including airspace and airport operation, combining data-driven analysis, mathematical models, and simulation studies, she works to realize even more resilient air traffic operation. She joined several academic and administrative communities as a committee and/or an advisory member, including the International Council of the Aeronautical Sciences (ICAS), the ICAO Surveillance Panel, the Airborne Surveillance Working Group, and the Science Council of Japan. She was a recipient of the McCarthy Award, in 2006, the John J. Green Award from the ICAS, in 2010, and the Distinguished Service Award from the Air Traffic Control Association, Japan, in 2019.

KOZO FUJII (Member, IEEE) received the Ph.D. degree in engineering from The University of Tokyo, Tokyo, Japan, in 1980.

From 1981 to 1983, he was a NRC Research Associate at NASA's Ames Research Center, USA. He was a Senior Research Scientist at the National Aerospace Laboratory, Chofu, Japan, from 1984 to 1988. He was an Associate Professor with the Institute of Space and Astronautical Science, Japan Aerospace Exploration Agency (ISAS/JAXA), Sagamihara, Japan, from 1988 to 1997, where he was a Professor, from 1997 to 2015. Since April 2015, he has been a Professor at the Tokyo University of Science, Tokyo. His research interests include aero-acoustics and flow control. He has been a Fellow of the AIAA, since 2004. He is one of the 210 members of the Science Council of Japan. He received many awards, such as the Daniel and Florence Guggenheim Award from the International Council of the Aeronautical Sciences (ICAS), in 2004. He served as the editorial board member of many journals.